

# Quartz-enhanced photoacoustic spectroscopy exploiting low-frequency tuning forks as a tool to measure the vibrational relaxation rate in gas species

Stefano Dello Russo<sup>a,b</sup>, Angelo Sampaolo<sup>b</sup>, Pietro Patimisco<sup>b</sup>, Giansergio Menduni<sup>b,c</sup>, Marilena Giglio<sup>b</sup>, Christine Hoelzl<sup>d</sup>, Vittorio M.N. Passaro<sup>c</sup>, Hongpeng Wu<sup>a</sup>, Lei Dong<sup>a,\*</sup>, Vincenzo Spagnolo<sup>a,b,\*</sup>

<sup>a</sup> State Key Laboratory of Quantum Optics and Quantum Optics Devices, Institute of Laser Spectroscopy & Collaborative Innovation Center of Extreme Optics, Shanxi University, Taiyuan 030006, China

<sup>b</sup> PolySense Lab, Dipartimento Interateneo di Fisica, University and Politecnico of Bari, CNR-IFN, Via Amendola 173, Bari, 70126 Italy

<sup>c</sup> Photonics Research Group, Dipartimento di Ingegneria Elettrica e dell'Informazione, Politecnico di Bari, Via Orabona 4, Bari, 70126, Italy

<sup>d</sup> Thorlabs GmbH, Münchner Weg 1, 85232 Bergkirchen, Germany

## ARTICLE INFO

### Keywords:

Quartz enhanced photoacoustic spectroscopy  
Quartz tuning forks  
Gas relaxation rate  
Methane  
Water vapour

## ABSTRACT

We demonstrated that quartz-enhanced photoacoustic spectroscopy (QEPAS) is an efficient tool to measure the vibrational relaxation rate of gas species, employing quartz tuning forks (QTFs) as sound detectors. Based on the dependence of the QTF resonance frequency on the resonator geometry, a wide range of acoustic frequencies with narrow detection bandwidth was probed. By measuring the QEPAS signal of the target analyte as well as the resonance properties of different QTFs as a function of the gas pressure, the relaxation time can be retrieved. This approach has been tested in the near infrared range by measuring the CH<sub>4</sub> ( $\nu_4$ ) vibrational relaxation rate in a mixture of 1% CH<sub>4</sub>, 0.15 % H<sub>2</sub>O in N<sub>2</sub>, and the H<sub>2</sub>O ( $\nu_1$ ) relaxation rate in a mixture of 0.5 % H<sub>2</sub>O in N<sub>2</sub>. Relaxation times of 3.2 ms Torr and 0.25 ms Torr were estimated for CH<sub>4</sub> and H<sub>2</sub>O, respectively, in excellent agreement with values reported in literature.

## 1. Introduction

Quartz-enhanced photoacoustic spectroscopy (QEPAS) has been widely used for trace gas sensing applications due to its high sensitivity and selectivity, and the very small volumes required [1–5]. QEPAS is based on the detection of sound waves generated by absorption of modulated optical radiation from gas target molecules. The sound detector is a piezoelectric quartz tuning fork (QTF) which converts small deflections of the prongs generated by the pressure waves into an electrical signal. The excited QTF in-plane flexural resonance modes are characterized by a high-quality factor as well as high immunity to environmental acoustic noise [6,7]. A crucial aspect in QEPAS detection is the dependence of the QEPAS signal on the radiation-to-sound conversion efficiency, which affects the acoustic waves generation within the gas. It is mainly determined by the transfer rate of the vibrational energy of excited analyte molecules into kinetic energy (translation) of

the surrounding molecules (V-T relaxation) [8]. Starting from 2002 [1], standard QTFs operating at a frequency as high as 32.7 kHz were commonly used for QEPAS sensing. In relation to this frequency, the gas species can be categorized in two groups, fast and slow relaxing gases, usually referring to relatively low concentrations (ppm range or lower) of the absorbing analyte in a matrix of inert gas, typically N<sub>2</sub>. For slow relaxing molecules, the 32.7 kHz laser modulation frequency is significantly higher than the effective analyte relaxation rate in the gas matrix, not allowing a complete release of the absorbed energy during each oscillation period. Thereby, the realization of custom QTFs with resonance frequencies of <32.7 kHz paved the way to the efficient detection of slow-relaxing molecules concentration leading to improved sensitivity levels [7,9–12]. Conversely, for fast relaxing gas species, the relaxation rate is significantly faster than the optical modulation frequency and an efficient energy transfer occurs between absorbing molecules and surrounding gas matrix during each oscillation period

\* Corresponding authors at: State Key Laboratory of Quantum Optics and Quantum Optics Devices, Institute of Laser Spectroscopy & Collaborative Innovation Center of Extreme Optics, Shanxi University, Taiyuan 030006, China.

E-mail addresses: [donglei@sxu.edu.cn](mailto:donglei@sxu.edu.cn) (L. Dong), [vincenzoluigi.spagnolo@poliba.it](mailto:vincenzoluigi.spagnolo@poliba.it) (V. Spagnolo).

<https://doi.org/10.1016/j.pacs.2020.100227>

Received 11 June 2020; Received in revised form 21 October 2020; Accepted 3 December 2020

Available online 9 December 2020

2213-5979/© 2020 The Authors.

Published by Elsevier GmbH. This is an open access article under the CC BY-NC-ND license

(<http://creativecommons.org/licenses/by-nc-nd/4.0/>).

[13]. However, the effective relaxation rate of a target gas depends on the surrounding matrix composition. Therefore, fast relaxing gases (such as H<sub>2</sub>O and SF<sub>6</sub>) can be added in the gas matrix to act as relaxation promoters, thereby enhancing the target analyte relaxation rate and the QEPAS detection sensitivity [14–16]. In this case, the excited target molecules can relax in different channels through collisions with the different types of molecules composing the matrix, including both the buffer and the promoter. The relaxation rate is then given by the sum of the relaxation rates of every possible energy transfer pathway, weighted by the concentration of each species in the mixture [17,18]. However, since the slow-relaxing gas QEPAS signal depends on the promoter concentration within the mixture, the promoter concentration has to be detected and monitored, increasing the complexity of the sensing systems. This issue has been addressed by exploiting the capability of QTFs to simultaneously operate at two different vibrational modes [19]. The QTF flexural 1st overtone mode can be excited along with the fundamental one, allowing simultaneous dual-gas QEPAS detection of target and relaxation promoter gas species via frequency division multiplexing (FDM) technique [20,21].

The influence of V-T relaxation rate on photoacoustic signal was first investigated in 1996 by Repond and Sigrist [22], studying its dependence on fundamental thermodynamic parameters, namely the pressure and the temperature. In 2006, Wysocki et al. [23] studied the vibrational relaxation rate on a QEPAS sensor employing a 32.7 kHz-QTF. In this work, the amplitude and phase of the QEPAS signal of CO<sub>2</sub> at a fixed concentration are analyzed as a function of the concentration of H<sub>2</sub>O vapor, acting as V-T promoter. The obtained results highlight the possibility of estimating absolute relaxation rate, which is the relaxation time of a molecule on itself, starting from known concentrations of the molecules in the mixture, but the evaluation of the effective relaxation rate of an unknown gas sample is not feasible. However, a QTF frequency as high as 32.7 kHz is not appropriate for a slow relaxing gas like CO<sub>2</sub>. In general, an accurate estimation of the gases vibrational relaxation rate can only be performed by exploiting different quartz tuning forks having resonance frequencies in a wide frequency range, in order to comprehensively investigate both slow and fast relaxing gases.

Therefore, the experimental apparatus conceived in the present work implements a QEPAS sensor with interchangeable QTFs, whose resonance frequencies range from 3 kHz to 45 kHz, to measure the effective relaxation time of a slow relaxing analyte (methane) and a fast one (H<sub>2</sub>O vapor). Two diode lasers, one resonant with a CH<sub>4</sub> absorption line located at 6046.96 cm<sup>-1</sup> and one targeting an H<sub>2</sub>O absorption line at 7226.02 cm<sup>-1</sup> have been used as the light sources to generate QEPAS signals. For each QTF and respective resonance mode, the CH<sub>4</sub> and H<sub>2</sub>O QEPAS signals, as well as the quality factor of the QTFs have been measured as a function of pressure. Thus, the radiation-to-sound conversion efficiency trends have been reconstructed as a function of pressure, for different acoustic frequencies. The analysis of these trends allowed the estimation of the effective relaxation rates for both gas species.

## 2. Classical theory on vibrational relaxation rate

A fundamental vibration is activated when a molecule in its ground state absorbs a quantum of energy. The molecule can be deactivated by emitting a photon or colliding with surrounding molecules. Since the radiative lifetime for infrared radiation is long (usually between 10<sup>-1</sup> and 10<sup>-3</sup> s), this mechanism can be neglected. Thus, the molecule mainly loses vibrational energy through collisions with its nearest neighbors. Landau [24] proposed a theoretical model to consider a collision between a vibrating molecule and a non-vibrating one. The model is based on the elementary kinetic theory, in which molecules are treated as hard spheres with a finite collision diameter. It supposes a  $\nu(1 \rightarrow 0)$  transfer when a molecule in the  $\nu = 1$  state collides with another molecule in the  $\nu = 0$  state. All other non-excited molecules are supposed to be in the state  $\nu = 0$  and a Boltzmann distribution is assumed to rule

the population between two levels. With these assumptions, the relaxation time  $\tau$  is introduced, which is proportional to the inverse of the number of collisions suffered by one molecule per second. Since the rate collision is proportional to the number of molecules in a given volume, and hence to the gas pressure  $P$ ,  $\tau$  is inversely dependent on  $P$ . Thus, the relaxation time is expressed as the inverse of the product between a rate constant  $k$  and  $P$ . In other words,  $\tau$  represents the V-T relaxation time, i. e. the time required to transfer the vibrational energy of the excited molecule into kinetic energy (translation) of the surrounding ones. These V-T energy transfer processes result in a heat production rate. Analyses based on level population are widely adopted. The molecule density  $N_{tot}$  of the absorbing gas is modelled by a two-level system, consisting of a vibrational ground state having molecule density  $N$  and an excited state with molecule density  $N'$ . In the approximation that  $N' \ll N$ , the rate equation for  $N'$  is given by:

$$\frac{dN'}{dt} = N\sigma\Psi - \frac{N'}{\tau} \quad (1)$$

where  $\Psi$  and  $\sigma$  denote the photon flux and the absorption cross-section, respectively. Radiative relaxation time and stimulated emission from the excited state have both been neglected. For a harmonic modulation at frequency  $f$  of the photon flux  $\Psi = \Psi_0(1 + e^{i2\pi ft})$ , periodic heating occurs in the sample, generating pressure waves. The frequency-dependent QEPAS signal generated at the modulation frequency  $f$  will be given by:

$$S = KQ(P)P_L I_{2f}(P) \varepsilon(f, \tau(P)) = \frac{KQ(P)P_L I_{2f}(P)}{\sqrt{1 + [2\pi f \tau(P)]^2}} \quad (2)$$

where  $K$  is a sensor constant,  $Q(P)$  is the QTF quality factor and  $P_L$  is the laser power,  $I_{2f}(P)$  is the peak intensity of the second-derivative of the absorption line simulated by HITRAN database (as usually obtained when operates in wavelength-modulation and 2f-detection [25]) and  $\varepsilon(f, \tau(P))$  is the radiation-to-sound conversion efficiency, given by:

$$\varepsilon[f, \tau(P)] = \frac{1}{\sqrt{1 + [2\pi f \tau(P)]^2}} \quad (3)$$

where  $\tau$  can be expressed as:

$$\tau = \frac{1}{kP} \quad (4)$$

For instantaneous relaxation, i.e.  $2\pi f \tau \ll 1$ ,  $\varepsilon = 1$  and the QEPAS signal is independent on the modulation frequency.

## 3. Methane relaxation rate in standard air

Methane QEPAS sensors reported in literature often investigated gas mixtures of methane in an N<sub>2</sub>-H<sub>2</sub>O matrix [6]. Water vapor is added to N<sub>2</sub> buffer to increase the CH<sub>4</sub> QEPAS signal because its V-T relaxation rates are several orders of magnitude faster than those of other molecules with comparable energy levels, but not hydrogen bonded. This is because water presents a wide absorption spectrum and is a polar molecule [26,27]. Several works demonstrated the linear increment of the CH<sub>4</sub> photoacoustic signal with the water content, when the CH<sub>4</sub> concentration is below 1% [8,20,28,29]. N<sub>2</sub> molecules are high-density collisional partners for excited CH<sub>4</sub> molecules. The presence of H<sub>2</sub>O in the gas mixture opens an additional relaxation path. Thus, all energy transfer paths in the CH<sub>4</sub>-N<sub>2</sub>-H<sub>2</sub>O gas mixture contribute to the relaxation process from the excited analyte state. The vibrational modes of methane include two bending modes,  $\nu_2$  (1533 cm<sup>-1</sup>) and  $\nu_4$  (1311 cm<sup>-1</sup>), and two stretching modes  $\nu_1$  (2917 cm<sup>-1</sup>) and  $\nu_3$  (3019 cm<sup>-1</sup>). The two stretching mode wavenumbers are approximately twice the bending mode ones, leading to a distribution of the vibrational levels in polyads. When the methane is optically excited in the near-infrared range at 6038 cm<sup>-1</sup>, the  $2\nu_3$  level is excited in the P4-Tetradecad. The

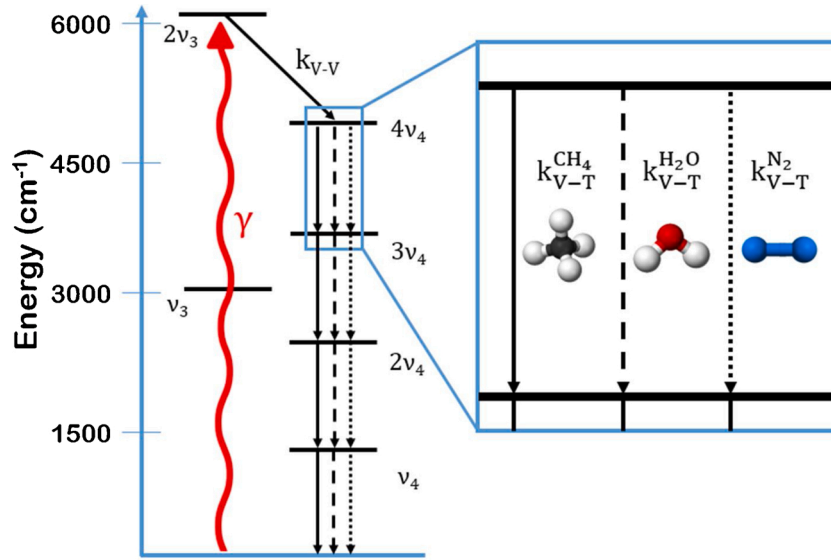


Fig. 1. Energy-level diagram of  $\text{CH}_4$  molecule, showing the laser excitation ( $\gamma$ ) to the  $2\nu_3$  state and the subsequent preferential relaxation scheme.

schematic of the energy transitions involved is shown in Fig. 1.

Due to the strong interactions existing between the states in P4-Tetradecad, very fast energy transfers (in the nanosecond range) occur between  $2\nu_3$  and  $4\nu_4$ , which is the lowest level of P4-Tetradecad, via vibrational-to-vibrational processes. Then, the energy transfer between consecutive polyads essentially occurs via the exchange of one  $\nu_4$  vibrational quantum via V-T relaxation processes with all collisional partners [17]. Therefore, a rate constant can be introduced for each collisional partner, namely  $k_{\text{H}_2\text{O}}$ ,  $k_{\text{N}_2}$  and  $k_{\text{CH}_4}$ . In this way, the relaxation time of  $2\nu_3$  excited state of  $\text{CH}_4$  is given by a weighted sum of the relaxation rates corresponding to collisions with the different types of neighbor molecules ( $\text{H}_2\text{O}$ ,  $\text{N}_2$  and  $\text{CH}_4$  itself), and taking into account the concentration of each species:

$$k = k_{\text{H}_2\text{O}}C_{\text{H}_2\text{O}} + k_{\text{N}_2}C_{\text{N}_2} + k_{\text{CH}_4}C_{\text{CH}_4} \quad (5)$$

being  $C_{\text{H}_2\text{O}}$ ,  $C_{\text{N}_2}$  and  $C_{\text{CH}_4}$  the concentration of  $\text{H}_2\text{O}$ ,  $\text{N}_2$  and  $\text{CH}_4$ , respectively. The rate constants are provided in literature and summarized in the following table.

Methane collisions with water have a rate constant two orders of magnitude higher than with  $\text{CH}_4$  and three orders of magnitude higher than with  $\text{N}_2$ . If the concentration of the three gas components are known, the effective relaxation time of methane in the gas matrix can be calculated.

#### 4. Experimental investigation

The estimation of vibrational relaxation rates will be obtained by measuring the radiation-to-sound conversion efficiency. However, both the QTF quality factor  $Q$  and  $\epsilon$  are pressure-dependent. When the gas pressure varies, Eq. (2) shows that the ratio  $S(P)/[Q(P) \cdot I_2(P)]$  follows the same trend as  $\epsilon$ . In addition,  $\epsilon$  depends on the sound frequency, i.e. on the QTF resonance frequency, at the selected flexural mode. Thus, for different QTFs and excited modes, a family of  $\epsilon_i$  functions is expected. In order to perform this investigation, a set of five QTFs was selected: six flexural resonance modes were excited in order to have a suitable frequency span from 3 kHz up to 44 kHz. In Table 2, selected QTFs are

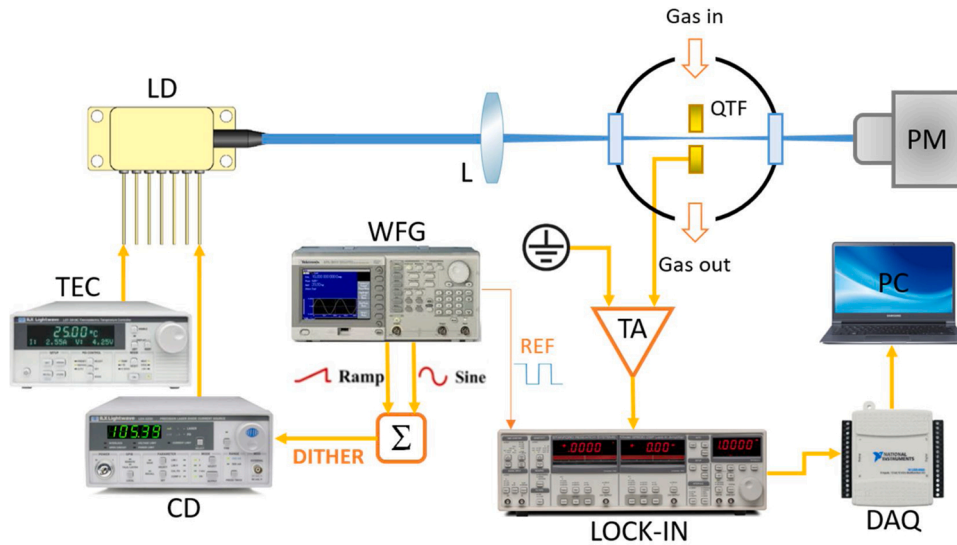


Fig. 2. Experimental setup for relaxation rate measurements with custom QTFs optimized for QEPAS sensing. LD: Laser diode, TEC: Thermoelectric cooler, CD: Current driver, WFG: Waveform generator, TA: Trans-impedance amplifier, L: Focusing lens, DAQ: Data acquisition card, PM: Power meter, REF: TTL reference signal,  $\Sigma$ : Adder.

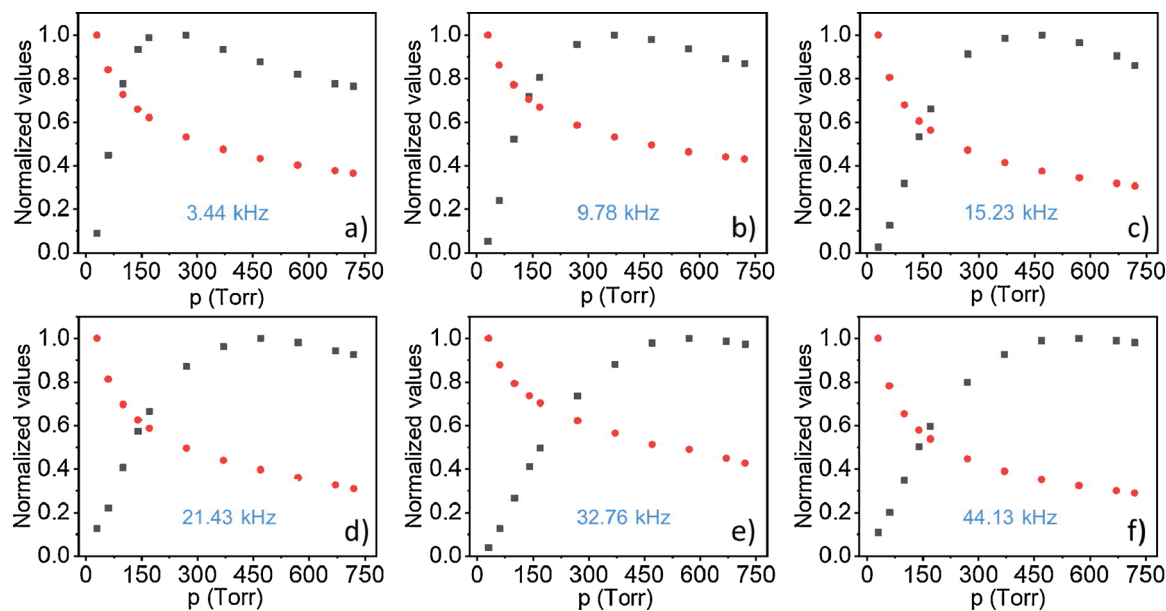


Fig. 3. Normalized QEPAS methane peak signal (black squares) and QTF quality factor (red dots) obtained with a set of 5 QTFs operating at selected flexural modes (as per Table 2), for a mixture of 1% CH<sub>4</sub>, 0.15 % H<sub>2</sub>O and 98.85 % N<sub>2</sub>. The frequency of each resonance mode is reported in blue.

labelled and the frequencies of the selected resonance modes are reported. QTFs' geometry and prong sizes are described in detail in the references listed in the leftmost column.

The quality factor of each resonance mode has been evaluated by acquiring the QTF resonance curve as a response to an electrical excitation. A function generator (Tektronix model AFG3102) was used to provide a sinusoidal voltage as excitation signal to the QTFs. The generated piezocurrent is converted into a voltage signal by using a transimpedance amplifier. The output voltage is demodulated by a lock-in amplifier (Stanford Research Model SR830) at the excitation frequency. By gradually varying the excitation frequency, the resonance curve is reconstructed. The ratio between the peak frequency and the full-width-half-maximum value of the resonance curve provides an estimation of the quality factor. All QTFs have been mounted in a stainless-steel enclosure in order to fix and control the gas pressure. The investigated pressure range was 30–760 Torr.

The setup for generating the QEPAS signal is depicted in Fig. 2.

A single-mode continuous-wave pigtailed diode laser was used as CH<sub>4</sub> excitation source to generate QEPAS signals. With an optical power of 14 mW, the diode laser targets a methane absorption line located at 6046.96 cm<sup>-1</sup>, having line strength of 1.46·10<sup>-21</sup> cm/molecule [32]. The laser was coupled with a fiber collimator whose output beam was focused between the QTF prongs using a lens with a focal length of 50 mm. A stainless-steel enclosure equipped with two near-IR windows was realized in order to accommodate and easily interchange QTFs. A certified gas mixture composed of 1% of CH<sub>4</sub>, 0.15 % of H<sub>2</sub>O and nitrogen as rest was used as test mixture. A flow-rate controller fixed the gas flow rate to 20 sccm, while a pressure controller, a valves system and a pump (not shown in Fig. 2) stabilized the gas pressure within the enclosure to a selected value. The QEPAS sensor operated with a wavelength modulation and dual-frequency detection approach, i.e. the laser beam was wavelength-modulated at half of the selected resonance mode frequency providing an external sinusoidal oscillation to the current driver, while the lock-in amplifier demodulated the signal at the resonance mode frequency. A QEPAS scan across the absorption line was acquired by applying a slow ramp to the current driver. The laser beam waist in the lens focal plane, i.e. between QTF prongs, was measured by using an infrared pyrocamera (Ophir, Spiricon) and it was ~200 μm, well below the smallest employed prongs spacing (300 μm for QTF#4). As a result, more than 99 % of the laser optical power passed through

QTF prongs without touching them.

## 5. Measurement of methane relaxation rate in nitrogen/water mixture

A QEPAS scan of the selected methane absorption line was acquired for eleven pressure values in the range 30–760 Torr. For each gas pressure, the peak-to-peak amplitude as well as frequency of the current modulation were adjusted in order to maximize the peak value of the QEPAS scan. Indeed, the amplitude modulation is related to the full width at half maximum (FWHM) value of the absorption line, which depends on the pressure broadening.  $I_{2f}$  (see Eq. (2)) is pressure-dependent and proportional to the product between the second derivative of the absorption coefficient peak and the squared modulation amplitude of the emission frequency [25]. However, considering the experimental modulation depths optimizing the QEPAS signals and the absorption coefficient values provided by the HITRAN database [32], it has been verified that the  $I_{2f}$  dependence on pressure can be neglected, as it provides a nearly constant value. The QTF resonance frequency is also pressure-dependent and it linearly decreases when the pressure increases. Then, peak values of each QEPAS scan have been extracted, for all the resonance modes reported in Table 2. Fig. 3 depicts the quality factor and the QEPAS peak signal trends as a function of pressure when the certified gas mixture is flowing through the acoustic detection module. In order to make the comparison more effective, all the data have been normalized to their respective peak values.

For each resonance mode, the quality factor monotonically decreases as the pressure increases. This is due to the gas surrounding the QTF, which acts as a damper for the prong vibrations. Gas damping is the main loss mechanism for the fundamental and first overtone mode and it is proportional to the viscosity and density of fluid. A good approximation for the dependence of the quality factor on the gas pressure is provided by the following equation [33,34]:

$$Q(P) = \frac{Q_0}{1 + Q_0 b \sqrt{P}} \quad (6)$$

where  $Q_0$  is the quality factor at  $P = 0$ , which includes all pressure-independent loss mechanisms (support losses and thermoelastic damping), and  $b$  is a fitting parameter. Both  $Q_0$  and  $b$  are mainly related to QTF geometry and gas viscosity, thus vary for each QTF. Starting from  $P = 30$

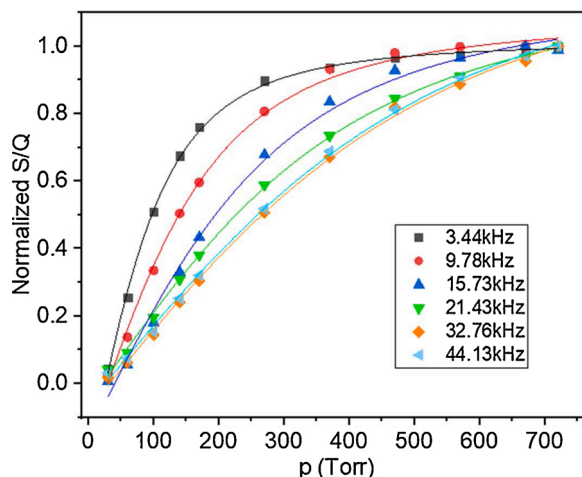


Fig. 4. Normalized  $S/Q$  of methane on a mixture of 1%  $\text{CH}_4$ , 0.15 %  $\text{H}_2\text{O}$  and 98.85 %  $\text{N}_2$  for all the resonance modes investigated. The lines represent the best fit using Eq. (7).

Torr, the QEPAS signal rapidly increases until it reaches a maximum value; then it slightly decreases. When the pressure decreases, the QTF quality factor increases while the number of molecules decreases, negatively affecting the radiation-to-sound conversion efficiency (see Eqs. (2) and (3)). Conversely, at high pressures a larger number of molecules guarantees an efficient sound generation but the QTF quality factor is lower. Thus, the maximum point in the graph of the QEPAS signal corresponds to the pressure value at which the tradeoff between the opposite behaviors of  $\epsilon$  and  $Q$  occurs. This tradeoff pressure varies with the modulation frequency. This is expected because the radiation-to-sound conversion efficiency depends on the sound frequency (see Eq. (3)). The maximum point in the QEPAS signal versus pressure dependence is more distinct at frequencies below 21 kHz, where it occurs at comparably low pressures. For  $f=32.76$  kHz and 44.13 kHz the QEPAS signal reaches its maximum value around  $\sim 500$  Torr: above that, the QEPAS signal remains almost unchanged. This aspect is crucial for studying the vibrational relaxation time of  $\text{CH}_4$  in the gas mixture and can be better understood by analyzing the radiation-to-sound conversion efficiency as a function of the resonance frequency. As discussed, this study can be carried out in terms of the ratio between the QEPAS signal and the quality factor. Thereby, for each resonance modes, the ratio  $S/Q$  is reported in Fig. 4 as a function of the investigated pressure values (data points).

For each frequency, the ratios  $S/Q$  have been normalized to the corresponding maximum values. The results reveal the strong dependence of  $S/Q$  on the sound frequency. At the lowest investigated frequency (3.44 kHz),  $S/Q$  reaches the plateau level at  $P=400$  Torr and then remains almost constant up to atmospheric pressure. As the frequency increases, the plateau level is reached at higher pressures. However, for 32.76 kHz and 44.13 kHz, the plateau level is not reached, suggesting that the maximum  $S/Q$  value should occur at pressures higher than the atmospheric one. Normalized  $S/Q$  values can be fitted by using the theoretical expression introduced for the radiation-to-sound conversion efficiency (see Eq. (3)), thus the fitting function has the form:

$$F(p) = \frac{z}{\sqrt{1 + (A/P)^2}} + w \quad (7)$$

where  $A = 2\pi f/k$ ,  $z$  and  $w$  are just fitting parameters.

The fits of experimental data are shown in Fig. 4 as solid lines. The resulting fitting parameters are listed in Table 3:

The  $A$  parameter, defined as the product between the sound frequency and the time constant  $\tau$ , rules the growth rate of the radiation-to-sound conversion efficiency as a function of pressure.  $z$  is the maximum

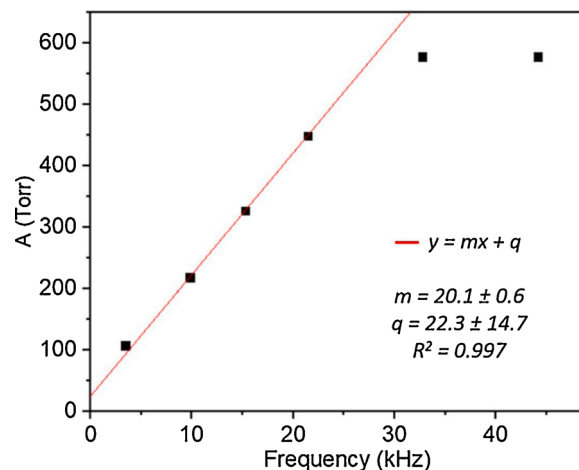


Fig. 5. Black squares: values of parameter  $A$  obtained by fitting on the experimental curves of the  $S/Q$  methane normalized ratio. Red line: linear fit performed on the first four values of the parameter  $A$ . The effective relaxation time constant results  $k^{-1} = m/2\pi$ , where  $m$  is the linear fit slope.

Table 1

V-T relaxation rates of the  $n^{\text{th}}$   $\nu_4$   $\text{CH}_4$  vibrational state with all collisional partners in the gas sample.

Reaction	Rate constant ( $\text{s}^{-1} \text{Torr}^{-1}$ )	Ref
$\text{CH}_4^*(n\nu_4) + \text{CH}_4 \rightarrow \text{CH}_4^*[(n-1)\nu_4] + \text{CH}_4$	$1.05 \cdot 10^3$	[30]
$\text{CH}_4^*(n\nu_4) + \text{N}_2 \rightarrow \text{CH}_4^*[(n-1)\nu_4] + \text{N}_2$	$1.05 \cdot 10^2$	[30]
$\text{CH}_4^*(n\nu_4) + \text{H}_2\text{O} \rightarrow \text{CH}_4^*[(n-1)\nu_4] + \text{H}_2\text{O}$	$1.32 \cdot 10^5$	[8]

Table 2

List of QTFs used in the analysis and related resonance frequencies.

#	Resonance mode	Frequency (kHz)	Ref.
QTF#1	Fundamental	3.44	[6]
QTF#2	Fundamental	9.78	[31]
QTF#3	Fundamental	15.23	[7]
QTF#1	First overtone	21.43	[6]
QTF#4	Fundamental	32.76	[1]
QTF#5	First overtone	44.13	[6]

value reachable when  $P$  tends to infinity. It can be noticed that for the QTFs with higher resonance frequency (32.76 kHz and 44.13 kHz)  $z$  tends to increase, validating the hypothesis that the investigation pressure range should be extended to pressures higher than the atmospheric one for reaching a plateau level. By fitting the  $A$  parameter as a function of the sound frequency, the rate constant can be retrieved by a linear fit. The results are shown in Fig. 5.

The trend shows a linear behavior of the  $A$  parameter as a function of frequency up to a cut-off value. The fitting procedure clearly underestimates the  $A$  parameter for 32.7 kHz and 44.1 kHz. This result, together with related comments above, demonstrates that sound frequencies greater than 30 kHz are not suitable to investigate the

Table 3

Fitting parameter obtained with Eq. (7) on the normalized methane  $S/Q$  experimental data.

Frequency (kHz)	$z$	$w$	$A$
3.44	1.26	-0.25	101
9.78	1.24	-0.17	220
15.23	1.3	-0.16	339
21.42	1.24	-0.06	459
32.76	1.37	-0.08	578
44.13	1.52	-0.07	576

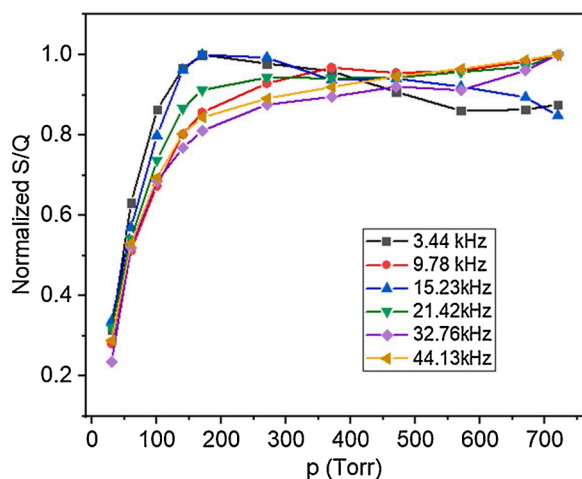


Fig. 6. Normalized  $S/Q$  of water vapor in a mixture of 0.5 %  $H_2O$  and 99.5 %  $N_2$  for all the resonance modes investigated. Solid lines are guides for eye.

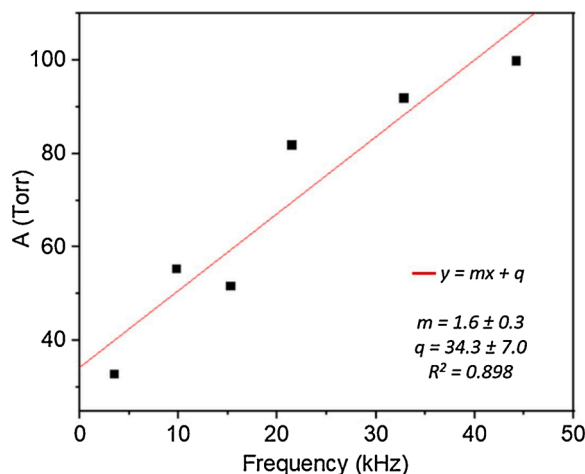


Fig. 7. Black squares: values of parameter  $A$  obtained by fitting on the experimental curves of the  $S/Q$  water vapor normalized ratio. Red line: linear fit performed on the values of the parameter  $A$ . The effective relaxation time constant results  $k^{-1} = m/2\pi$ .

vibrational relaxation time of the examined gas sample, at pressures lower than the atmospheric one. Therefore, a linear fit was imposed on data points related to the four lower frequencies, allowing an estimation of the  $CH_4$  effective relaxation time constant in the analyzed mixture  $k^{-1}$  of 3.2 ms Torr, with an uncertainty of 0.1 ms Torr. Considering the relaxation rate constants reviewed in Table 1, the effective time constant of the gas sample (1%  $CH_4$ , 0.15 %  $H_2O$  and 98.85 %  $N_2$ ) estimated via Eq. (5) is  $k^{-1}_{est} = 3.2$  ms Torr, in excellent agreement with the value extracted from the measurement data.

## 6. Measurement of water relaxation rate in nitrogen buffer

The robustness of the technique has been tested by targeting water vapor, a very fast relaxing molecule. In the experimental setup sketched in Fig. 2, the laser source has been replaced by a pigtailed laser diode with an optical power of 28 mW at  $7226.02\text{ cm}^{-1}$ , where the peak of a  $\nu_1$  water absorption line with linestrength of  $8.71 \cdot 10^{-21}\text{ cm}^2/\text{mol}$  is located [32]. A certified gas mixture with 0.5 % of water in  $N_2$  was used as test sample. By using the QTF resonance modes listed in Table 2 and following the same procedure described in Section 5, the QEPAS water peak signals and the QTF quality factors have been acquired at different pressure values of the gas flowing in the enclosure. The normalized

Table 4

V-T relaxation rates of the  $H_2O$  vibrational state with all collisional partners in the gas sample.

Reaction	Rate constant ( $s^{-1}\text{ Torr}^{-1}$ )	Ref
$H_2O^*(n\nu_1) + N_2 \rightarrow H_2O^*[(n-1)\nu_1] + N_2$	$1.32 \times 10^3$	[29]
$H_2O^*(n\nu_1) + H_2O \rightarrow H_2O^*[(n-1)\nu_1] + H_2O$	$7.00 \times 10^5$	[27]

ratios  $S/Q$  as a function of the pressure are reported in Fig. 6.

Starting from lower pressures,  $S/Q$  rapidly increases up to 200–300 Torr and then remains almost flat for higher pressure values, for all the investigated sound frequencies. This suggests that above 300 Torr the radiation-to-sound conversion efficiency of the water molecules in a nitrogen buffer is quite constant and it is almost independent on the excitation frequency. This is expected because of the fast vibrational-to-translation energy transfer of water molecules. Each curve has been fitted by using Eq. (7) and the  $A$  parameter has been extracted and plotted as a function of the frequency in Fig. 7.

The linear fit gives an estimation of the  $H_2O$  effective relaxation time constant  $k^{-1}$  of  $0.25 \pm 0.05$  ms Torr. A relative uncertainty as high as 20 % was obtained, about one order of magnitude higher than that obtained with the methane relaxation time ( $\sim 3\%$ ). This can be explained by the fact that the growth rate of  $S/Q$  functions with increasing pressure is almost the same for all investigated frequencies. Indeed, the relative relaxation time of water is known to be significantly lower than that of methane and the investigated frequency range should be increased towards higher frequencies. In this way, the measurement uncertainty could be improved. Despite the high measurement uncertainty, a comparison with the measurements reported in literature is instructive. Literature rate constants for  $H_2O \rightarrow H_2O$  and  $H_2O \rightarrow N_2$  relaxation pathways are summarized in the following table.

From the values listed in Table 4, the estimated effective relaxation time of the gas sample (0.5 %  $H_2O$  and 99.5 %  $N_2$ ) is  $k^{-1}_{est} = 0.21$  ms Torr, which corresponds to the experimental result within the uncertainty interval estimated with our approach.

## 7. Conclusions

In conclusion, the possibility to use the QEPAS technique to measure the vibrational relaxation rate of both slow and fast relaxing molecules in a defined gas matrix has been demonstrated. A QEPAS sensor implementing a set of QTFs whose resonance frequencies span from 3 kHz to 45 kHz has been employed to evaluate the  $CH_4$  non-radiative relaxation time in a gas sample composed of 1%  $CH_4$ , 0.15 %  $H_2O$  and 98.85 %  $N_2$ . The values of the  $CH_4$  radiation-to-sound conversion efficiency as a function of pressure were estimated by measuring the QEPAS signal and the QTF resonance mode quality factor. A relaxation time constant for  $CH_4$  of 3.2 ms Torr was extracted, in excellent agreement with the data present in literature. The same QEPAS sensor architecture was used to measure the relaxation time of water vapor in a mixture of 0.5 % of  $H_2O$  in nitrogen. A water relaxation time constant of 0.25 ms Torr was estimated, about an order of magnitude smaller than the value obtained with methane. This value is in good agreement with the results reported in literature. The obtained results demonstrate that QEPAS is an accurate and robust technique for energy relaxation rate measurements of gas species.

## Declaration of Competing Interest

The authors declare that there are no conflicts of interest.

## Acknowledgments

The authors from Dipartimento Interateneo di Fisica di Bari acknowledge the financial support from the European Union's Horizon 2020 research and innovation programme under the Marie Skłodowska-

Curie project OPTAPHI, grant No. 860808 and from THORLABS GmbH within the joint-research laboratory PolySense. Lei Dong acknowledge financial support by the National Natural Science Foundation of China (Grant Nos. 61805132), program TYMIT, Shanxi “1331KSC”, 111 project (D18001), Sanjin Scholar (No. 2017QNSJXZ-04), Applied basic research program of Shanxi Province (201801D221174), Scientific and Technological Innovation Programs of Higher Education Institutions In Shanxi (2019L0028).

## References

- [1] A.A. Kosterev, Y.A. Bakhrin, R.F. Curl, F.K. Tittel, Quartz-enhanced photoacoustic spectroscopy, *Opt. Lett.* 27 (2002) 1902–1904.
- [2] A. Sampaolo, S. Csutak, P. Patimisco, M. Giglio, G. Menduni, V. Passaro, F.K. Tittel, M. Deffenbaugh, V. Spagnolo, Methane, ethane and propane detection using a compact quartz enhanced photoacoustic sensors and a single interband cascade laser, *Sens. Actuators B Chem.* 282 (2019) 952–960.
- [3] M. Mordmueller, M. Koehring, W. Schade, U. Willer, An electrically and optically cooperated QEPAS device for highly integrated gas sensors, *Appl. Phys. B* 119 (2015) 111–118.
- [4] H. Wu, L. Dong, H. Zheng, Y. Yu, W. Ma, L. Zhang, W. Yin, L. Xiao, S. Jia, F. K. Tittel, Beat frequency quartz-enhanced photoacoustic spectroscopy for fast and calibration-free continuous trace-gas monitoring, *Nat. Commun.* 8 (2017) 15331.
- [5] X. Yin, H. Wu, L. Dong, B. Li, W. Ma, L. Zhang, W. Yin, L. Xiao, S. Jia, F.K. Tittel, Ppb-level SO<sub>2</sub> photoacoustic sensors with a suppressed absorption–Desorption effect by using a 7.41 μm external-cavity quantum cascade laser, *ACS Sens.* 5 (2020) 549.
- [6] P. Patimisco, A. Sampaolo, L. Dong, M. Giglio, G. Scamarcio, F.K. Tittel, V. Spagnolo, Analysis of the electro-elastic properties of custom quartz tuning forks for photoacoustic gas sensing, *Sens. Actuators B Chem.* 227 (2016) 539–546.
- [7] P. Patimisco, A. Sampaolo, M. Giglio, S. Dello Russo, V. Mackowiak, H. Rossmadl, A. Cable, F.K. Tittel, V. Spagnolo, Tuning forks with optimized geometries for quartz-enhanced photoacoustic spectroscopy, *Opt. Express* 27 (2019) 1401–1415.
- [8] A.A. Kosterev, Y.A. Bakhrin, F.K. Tittel, S. Mcwhorter, B. Ashcraft, QEPAS methane sensor performance for humidified gases, *Appl. Phys. B* 92 (2008) 103–109.
- [9] P. Patimisco, A. Sampaolo, H. Zheng, L. Dong, F.K. Tittel, V. Spagnolo, Quartz-enhanced photoacoustic spectrophones exploiting custom tuning forks: a review, *Adv. Phys. X* 2 (2016) 169–187.
- [10] F. Sgobba, G. Menduni, S. Dello Russo, A. Sampaolo, P. Patimisco, M. Giglio, E. Ranieri, V.M.N. Passaro, F.K. Tittel, V. Spagnolo, Quartz-enhanced photoacoustic detection of ethane in the Near-IR exploiting a highly performant spectrophone, *Appl. Sci.* 10 (2020) 2447.
- [11] M. Giglio, A. Elefante, P. Patimisco, A. Sampaolo, F. Sgobba, H. Rossmadl, V. Mackowiak, H. Wu, F.K. Tittel, L. Dong, V. Spagnolo, Quartz-enhanced photoacoustic sensor for ethylene detection implementing optimized custom tuning fork-based spectrophone, *Opt. Express* 27 (2019) 4271–4280.
- [12] S. Li, L. Dong, H. Wu, A. Sampaolo, P. Patimisco, V. Spagnolo, F. Tittel, Ppb-level quartz-enhanced photoacoustic detection of carbon monoxide exploiting a surface grooved tuning fork, *Anal. Chem.* 91 (2019) 5831–5840.
- [13] V. Spagnolo, P. Patimisco, S. Borri, G. Scamarcio, B.E. Bernacki, J. Kriesel, Part-per-trillion level SF<sub>6</sub> detection using a quartz enhanced photoacoustic spectroscopy-based sensor with single-mode fiber-coupled quantum cascade laser excitation, *Opt. Lett.* 37 (2012) 4461–4463.
- [14] A.A. Kosterev, Y.A. Bakhrin, F.K. Tittel, Ultrasensitive gas detection by quartz-enhanced photoacoustic spectroscopy in the fundamental molecular absorption bands region, *Appl. Phys. B* 80 (2005) 133–138.
- [15] V. Spagnolo, A.A. Kosterev, L. Dong, R. Lewicki, F.K. Tittel, NO trace gas sensor based on quartz-enhanced photoacoustic spectroscopy and external cavity quantum cascade laser, *Appl. Phys. B* 100 (2010) 125–130.
- [16] Y. Ma, R. Lewicki, M. Razeghi, F.K. Tittel, QEPAS based ppb-level detection of CO and N<sub>2</sub>O using a high power CW DFB-QCL, *Opt. Express* 21 (2013) 1008–1019.
- [17] S. Schilt, J.P. Besson, L. Thévenaz, Near-infrared laser photoacoustic detection of methane: the impact of molecular relaxation, *Appl. Phys. B* 82 (2006) 319–329.
- [18] M. Mordmueller, W. Schade, U. Willer, QEPAS with electrical co-excitation for photoacoustic measurements in fluctuating background gases, *Appl. Phys. B* 123 (2017) 224.
- [19] A. Sampaolo, P. Patimisco, L. Dong, A. Geras, G. Scamarcio, T. Starecki, F.K. Tittel, V. Spagnolo, Quartz-enhanced photoacoustic spectroscopy exploiting tuning fork overtone modes, *Appl. Phys. Lett.* 107 (2015), 231102.
- [20] H. Wu, X. Yin, L. Dong, K. Pei, A. Sampaolo, P. Patimisco, H. Zheng, W. Ma, L. Zhang, W. Yin, L. Xiao, V. Spagnolo, S. Jia, F.K. Tittel, Simultaneous dual-gas QEPAS detection based on a fundamental and overtone combined vibration of quartz tuning fork, *Appl. Phys. Lett.* 110 (2017), 121104.
- [21] A. Elefante, M. Giglio, A. Sampaolo, G. Menduni, P. Patimisco, V.M.N. Passaro, H. Wu, H. Rossmadl, V. Mackowiak, A. Cable, F.K. Tittel, L. Dong, V. Spagnolo, Dual-gas quartz-enhanced photoacoustic sensor for simultaneous detection of Methane/Nitrous oxide and water vapor, *Anal. Chem.* 91 (2019) 12866–12873.
- [22] P. Repond, M.W. Sigrist, Photoacoustic spectroscopy on trace gases with continuously tunable CO<sub>2</sub> laser, *Appl. Opt.* 35 (1996) 4065.
- [23] G. Wysocki, A.A. Kosterev, F.K. Tittel, Influence of molecular relaxation dynamics on quartz-enhanced photoacoustic detection of CO<sub>2</sub> at λ = 2 μm, *Appl. Phys. B* 85 (2006) 301.
- [24] L. Landau, Theory of sound dispersion, *Physikalische zeitschrift der Sowjetunion* 10 (1936) 34–43.
- [25] P. Patimisco, A. Sampaolo, Y. Bidaux, A. Bismuto, M. Scott, J. Jiang, A. Muller, J. Faist, F.K. Tittel, V. Spagnolo, Purely wavelength- and amplitude-modulated quartz-enhanced photoacoustic spectroscopy, *Opt. Express* 24 (2016) 25943–25954.
- [26] H.E. Bass, J.R. Olson, R.C. Amme, Vibrational relaxation in H<sub>2</sub>O vapor in the temperature range 373–946 K, *J. Acoust. Soc. Am.* 56 (1974) 1455–1460.
- [27] J. Finzi, F.E. Hovis, V.N. Panfilov, P. Hess, C.B. Moore, Vibrational relaxation of water vapor, *J. Chem. Phys.* 67 (1977) 4053–4061.
- [28] H. Wu, L. Dong, X. Yin, A. Sampaolo, P. Patimisco, W. Ma, L. Zhang, W. Yin, L. Xiao, V. Spagnolo, S. Jia, Atmospheric CH<sub>4</sub> measurement near a landfill using an ICL-based QEPAS sensor with V-T relaxation self-calibration, *Sens. Actuators B Chem.* 297 (2019), 126753.
- [29] N. Barreiro, A. Peuriot, G. Santiago, V. Slezak, Water-based enhancement of the resonant photoacoustic signal from methane–air samples excited at 3.3 μm, *Appl. Phys. B* 108 (2012) 369–375.
- [30] C. Boursier, J. Ménard, L. Doyennette, F. Menard-Bourcin, Rovibrational relaxation of methane in CH<sub>4</sub>–N<sub>2</sub> mixtures: time-resolved IR–IR double-resonance measurements at 193 K and kinetic modeling, *J. Phys. Chem. A* 107 (2003) 5280–5290.
- [31] Y. Ma, Y. He, P. Patimisco, A. Sampaolo, S. Qiao, X. Yu, F.K. Tittel, V. Spagnolo, Ultra-high sensitive trace gas detection based on light-induced thermoelastic spectroscopy and a custom quartz tuning fork, *Appl. Phys. Lett.* 116 (2020), 011103.
- [32] Hitran Database. Available online: <https://hitran.org/> (accessed on 1 May 2020).
- [33] P. Patimisco, A. Sampaolo, V. Mackowiak, H. Rossmadl, A. Cable, F.K. Tittel, V. Spagnolo, Loss mechanisms determining the quality factors in quartz tuning forks vibrating at the fundamental and first overtone modes, *IEEE Trans. Ultrason. Ferroelectr.* 65 (2018) 1951–1957.
- [34] M. Giglio, G. Menduni, P. Patimisco, A. Sampaolo, A. Elefante, V.M.N. Passaro, V. Spagnolo, Damping mechanisms of piezoelectric quartz tuning forks employed in photoacoustic spectroscopy for trace gas sensing, *Phys. Stat. Sol.* 216 (2019), 1800552.



**Stefano Dello Russo** obtained his M.S. degree (cum laude) in Physics in 2018 from the University of Bari. From the same year, he is a PhD student at the Physics Department of the University of Bari, developing his research work at PolySense Lab, joint-research laboratory between Technical University of Bari and THORLABS GmbH. Currently, his research activities are focused on the development of custom tuning forks for Quartz-Enhanced Photoacoustic Spectroscopy and on the study of vibrational-translational dynamics of molecules in gaseous mixtures.



**Angelo Sampaolo** obtained his Master degree in Physics in 2013 and the PhD Degree in Physics in 2017 from University of Bari. He was a visiting researcher in the Laser Science Group at Rice University from 2014 to 2016. Since May 2017, he is a Post-Doctoral Research associate at University of Bari. His research activity has included the study of the thermal properties of heterostructured devices via Raman spectroscopy. Most recently, his research interest has focused on the development of innovative techniques in trace gas sensing, based on Quartz-Enhanced Photoacoustic Spectroscopy and covering the full spectral range from near-IR to THz. His achieved results have been acknowledged by a cover paper in *Applied Physics Letter* of the July 2013 issue.



**Pietro Patimisco** obtained the Master degree in Physics (cum laude) in 2009 and the PhD Degree in Physics in 2013 from the University of Bari. Since 2018, he is Assistant professor at the Technical University of Bari. He was a visiting scientist in the Laser Science Group at Rice University in 2013 and 2014. Dr. Patimisco's scientific activity addressed both micro-probe optical characterization of semiconductor optoelectronic devices and photoacoustic gas sensors. Recently, his research activities included the study and applications of trace-gas sensors, such as quartz-enhanced photoacoustic spectroscopy and cavity enhanced absorption spectroscopy in the mid infrared and terahertz spectral region, leading to several publications, including a cover paper in *Applied Physics Letter* of the July 2013 issue.



**Giansergio Menduni** received the M.S. degree (cum laude) in Electronic Engineering in 2017 from the Technical University of Bari. Since 2018, he is a PhD student at the Electric and Information Engineering Department of the Technical University of Bari. His research activity is focused on the development of gas sensors based on Quartz Enhanced Photoacoustic Spectroscopy.



**Hongpeng Wu** received his Ph.D. degree in atomic and molecular physics from Shanxi University, China, in 2017. From September, 2015 to October, 2016, he studied as a joint Ph.D. student in the Electrical and Computer Engineering Department and Rice Quantum Institute, Rice University, Houston, USA. Currently he is a professor in the Institute of Laser Spectroscopy of Shanxi University. His research interests include gas sensors, photoacoustic spectroscopy, photothermal spectroscopy and laser spectroscopy techniques.



**Marilena Giglio** received the M.S. degree (cum laude) in Applied Physics in 2014, and the PhD Degree in Physics in 2018 from the University of Bari. In 2012 she's been visiting the Academic Medical Center of Amsterdam as a trainee. In 2015 she was a Research Assistant with the Department of Physics, University of Bari. She was a visiting researcher in the Laser Science Group at Rice University from 2016 to 2017. Since 2018, she is a Post-Doc Research Assistant at the Physics Department of the Technical University of Bari. Her research activity is focused on the development of gas sensors based on Quartz-Enhanced Photoacoustic Spectroscopy and on the optical coupling of hollow-core waveguides with interband- and quantum-cascade lasers.



**Lei Dong** received his Ph.D. degree in optics from Shanxi University, China, in 2007. From June, 2008 to December, 2011, he worked as a post-doctoral fellow in the Electrical and Computer Engineering Department and Rice Quantum Institute, Rice University, Houston, USA. Currently he is a professor in the Institute of Laser Spectroscopy of Shanxi University. His research interests include optical sensors, trace gas detection, photoacoustic spectroscopy and laser spectroscopy.



**Christine Hölzl** received the Dipl.-Phys. and Dr. rer. nat. degrees from Technical University Munich in 2006 and 2012, respectively. During her PhD thesis, her research interest was in the field of ultrafast optical orientation and time-resolved spectroscopy of carrier spin dynamics in semiconductor materials. Currently, she is contributing to the development of spectroscopy solutions at THORLABS GmbH.



**Vincenzo Spagnolo** obtained the PhD in physics in 1994 from University of Bari. From 1997–1999, he was researcher of the National Institute of the Physics of Matter. Since 2004, he works at the Technical University of Bari, formerly as assistant and associate professor and now as full Professor of Physics. Starting from 2019, he become Vice-Rector of the technical university of Bari - Deputy to Technology Transfer. He is the director of the joint-research lab PolySense between Technical University of Bari and THORLABS GmbH, fellow member of SPIE and senior member of OSA. His research interests include optoacoustic gas sensing and spectroscopic techniques for real-time monitoring. His research activity is documented by more than 210 publications and 3 filed patents. He has given more than 50 invited presentations at international conferences and workshops.



**Vittorio M.N. Passaro** is associate professor at Politecnico di Bari since 2000. Since 1988 his research interests are focused on modeling and design of integrated optical devices and circuits for optical signal processing, telecommunications and sensing. He has published more than 380 papers published in peer reviewed high impact journals and conference proceedings, with more than 3200 cites in Scopus database. Since 2012 Prof. Passaro is Editor-in-Chief of Sensors journal and since april 2020 he has been appointed as Associate Editor of Optics Express.